Management Strategies and Engineering Sciences 2025; 7(6):1-17

Calculation of the Ductility Factor (m) of Composite Columns Using Experimental Results and Finite Element Software

Seyyed Shahram Jafari[1], Shahriar Tavousi Tafreshi[1*]

[1] Department of Earthquake, Civil Engineering, CT.C., Islamic Azad University, Tehran, Iran

*** Corresponding author email address**: sh_tavousi@iauctb.ac.ir

Received: 2025-04-13 **Reviewed:** 2025-06-09 **Revised:** 2025-06-16 **Accepted:** 2025-06-29 **Published:** 2025-12-20

Abstract

This study investigates the deformation capacity factor (m) of composite columns using experimental data and finite element numerical modeling. The real behavior of these columns was analyzed using the Krawinkler–Ibarra cyclic loading protocol, and parameters such as deformation capacity, modified axial resistance, and hysteretic behavior were assessed to evaluate energy absorption ability. The research combines numerical analyses in finite element software and experimental results from concrete-filled steel tube (CFT) columns. Force-displacement curves under cyclic loading were extracted, and by identifying key points on the curve (yield, maximum, and failure points), the deformation capacity factor (m) was calculated according to the FEMA 356 guidelines and the Iranian code (publication 360). The results showed that the m factor for CFT sections ranges from 1.4 to 5.6, while for SRC sections, it ranges from 1.0 to 4.0. At axial loads exceeding 50% and 65% of the nominal capacity, respectively, the behavior of CFT and SRC sections shifts from deformation-controlled to force-controlled. Additionally, an empirical relationship for predicting axial load capacity was developed, improving the accuracy of predictions compared to common models. The findings indicate that CFT composite columns exhibit significant deformation capacity, and their m factor exceeds the values recommended in codes in most cases. This study contributes to a better understanding of the nonlinear behavior of composite columns and the optimization of seismic design, especially for retrofit projects.

Keywords: *Mathematical modeling of finite elements, Concrete-Filled Steel Tubes (CFT), Composite Columns, Ductility Factor (m), Cyclic Loading Behavior.*

How to cite this article:

Jafari, S. Sh., & Tavousi Tafreshi, Sh. (2025). Calculation of the Ductility Factor (m) of Composite Columns Using Experimental Results and Finite Element Software. Management Strategies and Engineering Sciences, 7(6), 1-17.

1. Introduction

Throughout history, humankind has always sought to build comfortable and safe shelters. Initially, this goal was achieved by observing and drawing inspiration from nature, as well as utilizing natural materials such as stone, wood, lime, adobe, and the like. With the discovery of metals, these valuable and useful materials, in combination with other natural resources, were increasingly employed in construction [1]. As the understanding and identification of construction materials evolved, and with the advent of cement in the early 19th century, the first concrete structures—composed of aggregates such as sand, gravel, and cement—were developed. However, it was soon recognized that plain concrete could only withstand compressive forces, while its tensile strength was approximately seven to fifteen times lower than its compressive capacity [2]. This realization led to the idea of incorporating steel reinforcement bars (rebars) to carry tensile stresses, giving rise to the development and proliferation of reinforced concrete structures [3].

Yet, the concept of combining materials and forming composite sections did not stop there. Over time, various structural systems utilizing composite sections were introduced and expanded. Examples include composite slabs made by combining steel beams with reinforced concrete, concrete-encased steel sections (either reinforced or unreinforced), concrete cores (reinforced or unreinforced)

embedded within steel profiles, and concrete sections (reinforced or unreinforced) confined using different types of fiber-reinforced polymers (FRPs), among others [4]. The primary rationale for combining materials in such composite sections is to compensate for the weaknesses of one material by leveraging the mechanical, thermal, or chemical advantages of another. For instance, as previously mentioned, the low tensile strength of concrete can be compensated by steel reinforcement or FRP sheets, while the shortcomings of steel elements—such as vulnerability to high temperatures, direct chemical corrosion, or local buckling—can be mitigated using concrete encasement [5].

As a result, the production and application of composite sections, along with extensive research aimed at better understanding their diverse behaviors under various types of applied loads and induced stresses, have increasingly attracted the attention of researchers and scholars in the field [6]. Composite sections have gained widespread attention and application among engineers due to their numerous structural and non-structural advantages. Given their increasing usage and growing prevalence in modern construction, it is essential to examine and elaborate on this subject in a comprehensive and detailed manner [7]. In recent decades, composite structural elements—particularly composite columns—have gained substantial attention in both new construction and seismic retrofitting applications due to their advantageous mechanical properties and economic efficiency [8]. These elements, which typically involve a combination of steel and concrete, exhibit superior strength, stiffness, and energy dissipation capacity when compared to their conventional counterparts. However, the complex interaction between the constituent materials introduces significant challenges in accurately predicting their structural behavior under various loading conditions [9]. Unlike traditional steel or reinforced concrete members, which benefit from decades of experimental research and well-established design codes, composite sections remain a subject of ongoing investigation. This is primarily due to the intricate interface behavior and non-linear interaction effects between steel and concrete, which influence key structural parameters such as load-bearing capacity, deformation patterns, failure modes, and especially ductility—a critical parameter in seismic design [10].

Although various international standards—including AISC (1999, 2005), ACI (1996), Eurocode (ENV1994), AIJ (1997), BCA (2005), and NZBC (1992)—have proposed design recommendations for composite elements, discrepancies between code-based predictions and experimental observations persist. In particular, the accurate evaluation of ductility coefficients for composite columns remains a major gap in both research and practice. Ductility plays a vital role in the assessment of structural resilience and directly influences the response modification factor (or behavior factor), which is central to performance-based seismic design [11].

This issue becomes even more critical in the context of retrofitting, where composite columns are often introduced to enhance the ductile behavior of existing structures. According to FEMA 356 and its Iranian equivalent, the Planning and Budget Organization's Publication No. 360, the ductility coefficient (denoted as m) is an essential input for capacity design, energy dissipation estimation, and performance evaluation. However, due to the lack of comprehensive parametric studies and reliable analytical models that reflect real behavior, the current understanding of ductility in composite columns remains limited. To address this challenge, the present study aims to evaluate the ductility coefficient (m) of composite columns using a combination of experimental data and finite element modeling. By applying standardized cyclic lateral loading protocols—specifically the one recommended by Krawinkler–Ibarra—this research seeks to:

1. Quantify the actual ductility capacity of composite columns;
2. Propose a correction factor for axial load-bearing capacity estimation;
3. Analyze hysteretic behavior to assess the energy dissipation potential

This work contributes to narrowing the gap between theoretical design methods and practical performance, and supports the development of more accurate and reliable design frameworks for composite columns in both new and retrofitted structures.

2. Literature Review

In recent years, composite columns have gained significant popularity, especially in high-rise structures and arch bridges, particularly in earthquake-prone regions such as China and Japan. This is largely due to the frequent seismic activity in these areas. The characteristics and advantages of composite columns, especially Concrete-Filled Tubes (CFT), are as follows:

1. **Optimized Material Properties**: In conventional composite structural systems, the interactive effects between steel and concrete allow the optimization

of the advantages of both materials, while minimizing their disadvantages. This synergy gives composite sections a distinct advantage over traditional systems like steel or reinforced concrete columns, making them a preferred choice for modern construction [12].

2. **Cost Reduction and Improved Performance**: Compared to conventional steel structures, the use of composite or dual systems can reduce costs. This reduction is primarily due to the decreased use of steel, increased stiffness from the higher moment of inertia of the sections, and improved fire resistance. These benefits make composite columns a cost-effective alternative with superior performance in comparison to conventional steel systems [13].
3. **Efficiency in Construction**: Steel tubes can be utilized as forms for concrete pouring and piling in buildings. Additionally, CFT structures offer significant advantages in construction efficiency compared to conventional reinforced concrete structures, primarily due to the elimination of the need for complex formwork and the faster assembly process [7].
4. **Development of Composite Columns**: The first composite columns were constructed using a type of steel column encased in concrete (Steel Reinforced Concrete: SRC). However, the main drawback of this type of composite column was the necessity for complete formwork and reinforcement cages to prevent the concrete core from cracking. In contrast, CFT columns do not face these issues, eliminating significant time and cost inefficiencies [14].

The key advantage of these composite sections is the interaction between steel and concrete, where concrete helps restrain and stabilize the steel, delaying local buckling in the steel section. Other benefits include increased ductility and high endurance under cyclic and reversed loading, improved strength-to-weight ratio, and higher stiffness-to-weight ratio compared to conventional reinforced concrete elements. Furthermore, these columns offer material savings, reduced construction time, better fire resistance, smaller deformations compared to conventional steel columns, and increased compressive strength of concrete (in CFT) due to the confining effect of the steel tube [15]. Composite columns can be classified into two main types based on the arrangement of the section, the location of concrete and steel, and the manner of their placement within the section. These two broad categories are:

2.1. Steel Sections Encased in Concrete (Placed Inside Concrete)

In this type of composite section, the steel section is placed inside the concrete, and in technical terminology, the steel section is enclosed by a concrete jacket. In this composite section, to control shear cracks (caused by torsion and shear) or principal transverse cracks (caused by bending perpendicular to the longitudinal axis of the member), depending on the thickness of the concrete jacket, both transverse steel reinforcement (stirrups) and longitudinal reinforcement are required (Figure 1).

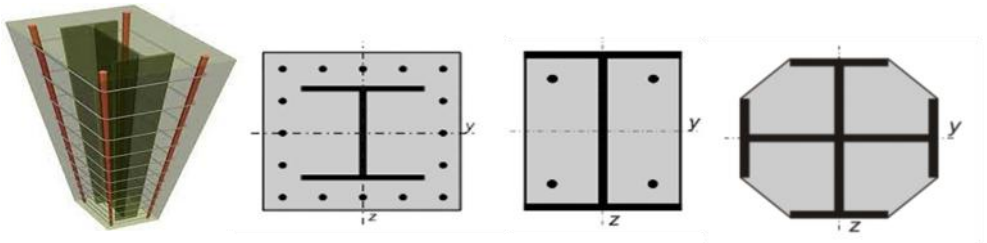

Figure 1. Types of S.R.C sections [2]

2.2. Concrete Encased by a Steel Section:

2.2.1. Concrete-Filled Steel Sections (C.F.T):

In these types of columns, the steel section plays a crucial role in bearing axial stresses caused by axial loads and bending moments, as well as resisting transverse stresses (shear) generated by shear forces or passive pressure resulting from concrete deformation (such as confinement stresses). This role is depicted in Figures 2 and 3. In technical literature, this type of composite section is referred to as Concrete-Filled Tube (C.F.T).

2.2.2. Tubular Columns:

Despite the fact that in C.F.T sections, the steel section serves for simultaneous axial and transverse reinforcement, in tubular columns, the steel section primarily serves a single function, unlike the more common C.F.T columns. In other words, the composite interaction between the steel tube and concrete is essentially considered only in the transverse direction in tubular columns, whereas, in conventional C.F.T columns, this interaction is considered in both the longitudinal (axial) and transverse (shear) directions. To achieve this, a gap is introduced between the lower flange of the beam and the steel section to prevent the transfer of vertical gravitational loads (live, dead, seismic, etc.) to this section. The steel tube thus only acts as a transverse reinforcement (Figures 2 and 3).

For example, in Thailand, one of the main applications of C.F.T sections is in the retrofitting of reinforced concrete columns that are deficient or structurally inadequate. These applications are typically aimed at enhancing and strengthening the resistance and ductility of these reinforced concrete sections against dead, live, wind, and seismic loads. However, due to a lack of comprehensive information on this type of secondary structural design for steel tube or C.F.T columns, such applications face limitations, making it a necessary area for further research, as highlighted in this study [1].

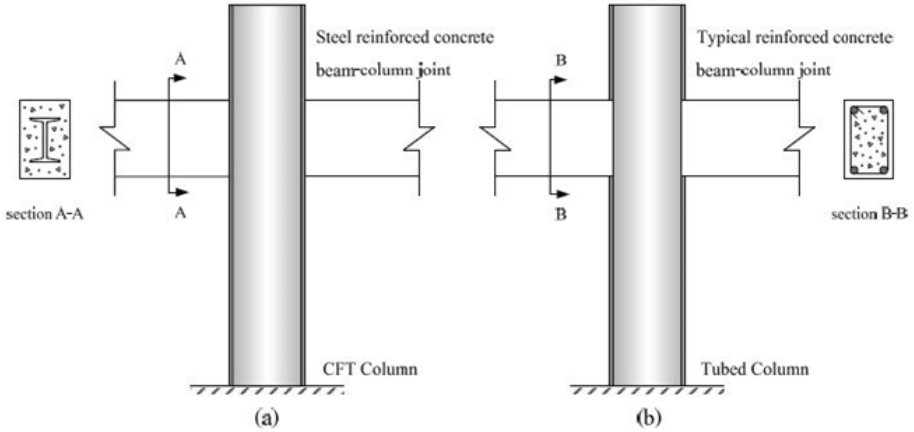

Figure 2. Two Types of Columns with C.F.T Composite Section [1].

Given the aforementioned points, composite columns possess numerous features and advantages that make them suitable for both primary design and as a form of retrofitting (secondary design). However, the key issue lies in the performance of these sections and the ductility coefficient that defines their behavior. In general, the response modification factor (or behavior factor) of a structure is a function of the ductility and performance of all its primary and secondary components [4].

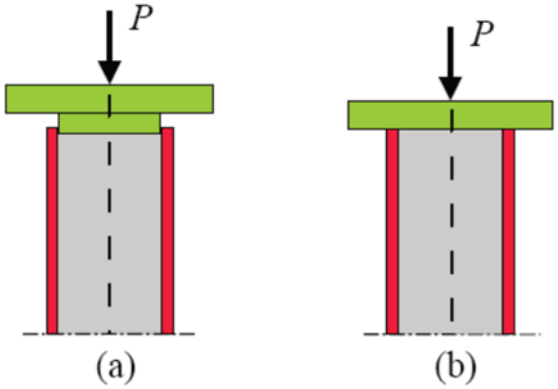

Figure 3. Schematic diagram of axial load application in C.F.T columns (a) and tubular columns (b).

In recent years, composite columns have gained significant popularity, especially in high-rise buildings and arch bridges, particularly in seismic-prone regions like China and Japan. Given the lack of technical information on this subject, numerous researchers have conducted studies on these types of sections due to their practical importance. Several renowned research associations from different countries have also conducted comprehensive studies on the behavior of these structural elements and have proposed design relationships for them. Some of the first comprehensive and finalized design codes include those published by AISC360 (American Institute of Steel Construction) in 1999 and 2005, ACI (American Concrete Institute) in 1996, Eurocode (ENV1994.1.1.2004), Architectural Institute of Japan (AIJ 1997), Building Code of Australia (BCA 2005), and New Zealand Building Code (NZBC 1992) [14].

the combined use of concrete and steel in the structure of sections was initially aimed at achieving fire resistance. After the composite action, which resulted from the strong bond between these materials, its impact on the structural resistance became evident. Consequently, extensive studies were conducted on the evaluation of composite action in sections. Research on C.F.T sections has continued for several decades [4]. The first use of C.F.T sections was recorded and published by Sewell in 1901, and the first comprehensive and complete experiments on C.F.T sections were conducted by Kloppel and Goder in 1957 [1]. The objective of Sewell's study on C.F.T sections was to address the protection of the hollow inner tube against corrosion due to rust. The role and effect of the added structural stiffness due to the composite section's behavior were observed when several columns were subjected to overload [15].

The development of studies on the axial resistance of C.F.T sections has continued since they were first tested by Kloppel and Goder. Sections with various shapes such as circular, square, and rectangular were also examined and tested. In the United Kingdom, C.F.T sections were first used in overpass bridges to carry heavy axial loads in the late 1870s. By the early 20th century, in 1915, Swain and Holmes were among the first to attempt to understand the behavior of these sections [2]. After these two, Kloppel and Goder conducted experiments on these sections, focusing on short columns with different slenderness ratios and various axial loads with eccentricities [16]. In 1970, Beer & Schulz conducted extensive theoretical and practical research on C.F.T sections, focusing mainly on geometric imperfections. Also, in Japan, the first code recommendations were issued by the Architectural Institute of Japan (AIJ) in 1967, which was revised in 1981 [9]. The tubular column system was developed to improve some of the shortcomings of conventional C.F.T columns, as written by Xiao in 2001 [1]. The idea of using steel as a primary and transverse reinforcement for reinforced concrete (RC) columns was initially studied by a research group led by Tomii [17].

2.3. Study of C.F.T Sections Columns

A column is a structural element primarily subjected to axial compression along its longitudinal axis. This element can be subjected to compressive force, or in combination with an eccentric load, bending moments, or a combination of these. The failure of short (stubby) compressed columns is caused by axial compressive forces, whereas in slender (tall) columns, the behavior and failure of compression members depend on both material strength and stiffness, as well as the geometry of the members [8]. The hollow steel section is a highly efficient structure for bearing compressive loads and is widely used in the frames of industrial buildings. However, steel is highly vulnerable to heat, which implies that a significant amount of steel is needed in design and construction. With the development of steel technology and construction, various methods have been developed to protect steel members, especially steel columns, against fire. Additionally, as construction technology has advanced, filling concrete into the hollow section is expected to not only increase the structural capacity but also improve the overall fire resistance of the member [18].

Several factors significantly affect the ultimate strength of C.F.T columns. These include the slenderness ratio, thickness of the steel section, the geometric shape of the section, and the mechanical properties of steel and concrete [19]. Generally, C.F.T members under axial compressive load can fail in two primary modes: slenderness failure and failure due to material properties. In short columns, material properties play a more significant role. Failure occurs when the steel section reaches the yielding point and the concrete fractures, which is the resistance criterion. On the other hand, the ultimate load-bearing capacity of slender C.F.T columns is limited by stability, where the members are likely to reach a critical state due to buckling and secondary effects. The critical buckling load is the load at which the section undergoes rapid, unstable deformations, typically governed by the section’s stiffness in slender sections, while in short (stubby) sections, the material properties and cross-sectional dimensions are more influential [20].

The shape of the column also contributes to its ultimate strength and behavior. Compared to open and hollow tube sections, the distribution of materials and the section's geometry, which is centered away from the cross-sectional axis, makes the hollow tube the most suitable for compression members. However, the disadvantage of these hollow tube sections is the difficulty in the connection of beams to the columns, requiring more advanced skills in construction. Today, various hollow tube sections are available in the market. Among them, the circular hollow section is significantly more efficient for applying compressive loads, as the moment of inertia, area, and stiffness are equal in all directions. Research has shown that the shape and thickness of the cross-section significantly affect the axial load resistance of C.F.T columns [21]. Based on these studies, it has been concluded that axially loaded circular C.F.T columns exhibit fully elastoplastic behavior, offering more axial ductility after yielding compared to square or rectangular C.F.T columns. Circular column behavior is largely governed by strain hardening, whereas post-yielding behavior in square and rectangular columns depends on the tube wall thickness [22].

3. Deformability Index Coefficient (m) in Composite Sections

the modification coefficient based on the nonlinear behavior of members (deformability index coefficient) is used to adjust the internal resistance forces generated in force-controlled members during linear analysis (static or dynamic linear). Since no building materials such as concrete and steel exhibit entirely linear behavior from the loading phase to failure, there is no perfectly linear, bilinear, or even trilinear relationship in the force-displacement (or moment-curvature) diagrams of these materials. Occasionally, to simplify, bilinear and trilinear diagrams are used, which introduce approximation and errors. Therefore, as stated earlier, in each of these diagrams, an acceptable approximation can be made with a coefficient to relate between the assumed linear behavior and the actual elastic-plastic behavior of the members [23].

Despite providing comprehensive data on the structural behavior of members under loading, cyclic loading diagrams are complex and difficult to generate, interpret, and analyze, which increases time and costs. Therefore, to obtain the force-displacement diagram of a member under lateral loading, two main methods are employed: incremental static loading (monotonic loading) and cyclic loading. The incremental static loading method also has disadvantages; important phenomena such as pinching, the Bauschinger effect, reversed loading, and cracking in concrete are not well modeled, and their effects are almost neglected. Therefore, to obtain an accurate force-displacement (moment-curvature) diagram of a member, it is recommended to apply cyclic loading, identify the peak points in each cycle, and connect them to derive the force-displacement diagram. In this derived diagram (from the peak points), the internal resistance forces (force or moment) are lower than the corresponding values obtained from the monotonic loading diagram, especially beyond the elastic range, and the corresponding deformations are also smaller [24].

Thus, to determine the value of the deformability index coefficient (m), the following steps must be followed:

1. Initially, according to Figure 4, points A, B, C, D, and E are identified on the force-displacement (moment-curvature) diagram.
2. Then, the ratio of these deformations to the yield deformation is calculated, which is indicated by the deformation at point B on the curve in Figure 4.
3. The result obtained in step 2 is then multiplied by 0.75 to derive the acceptable "m" coefficient [25].

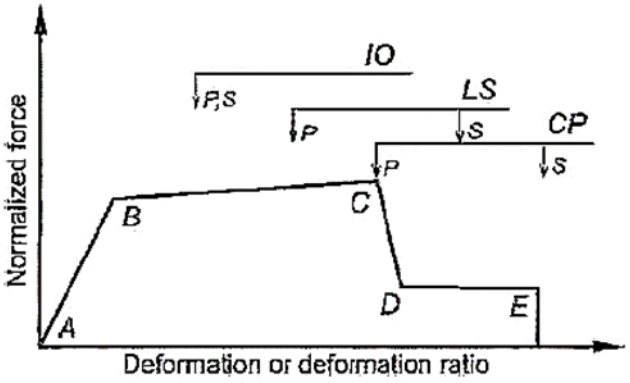

Figure 4. Image of FEMA 357 acceptance criteria [26].

3.1. *Deformation Corresponding to the Immediate Occupancy (I.O) Performance Level for Primary and Non-Primary Members*

The deformation at which visible and permanent damages were observed during experimental tests is used as the criterion for determining the deformation corresponding to this performance level. Specifically, the acceptable deformation corresponding to this state is 0.67 times the acceptable deformation associated with the Life Safety (L.S) performance level, as defined in the following clause.

3.2. *Deformation Corresponding to the Life Safety (L.S) Performance Level for Primary and Non-Primary Members*

a) Primary Members: 0.75 times the deformation corresponding to point C on the diagram presented in Figure 4.

b) Non-Primary Members: 0.75 times the deformation corresponding to point E on the diagram presented in Figure 4.

3.3. *Deformation Corresponding to the Collapse Prevention (C.P) Performance Level for Primary and Non-Primary Members*

a) Primary Members: The deformation corresponding to point C on the diagram shown in Figure 1, provided that this value does not exceed 75% of the deformation at point E.

b) Non-Primary Members: The deformation corresponding to point E on the diagram shown in Figure 1.

Table 1. Classification of members controlled by deformation based on performance levels

Performance Level	I.O – Immediate Occupancy	L.S – Life Safety	C.P – Collapse Prevention
Member Type	Primary (P) & Secondary (S)	Primary (P)	Secondary (S)
m Factor	m_1	m_2	m_3

$$m1 = 0.75 * 0.67 * (\frac{0.75*\Delta C}{\Delta B}) \quad (1)$$

$$m2 = 0.75 * (\frac{0.75 * \Delta C}{\Delta B}) \quad (2)$$

$$m3 = 0.75 * (\frac{0.75 * \Delta E}{\Delta B}) \quad (3)$$

$$m4 = 0.75 * (\frac{\min(0.75 * \Delta E \ \& \ \Delta C)}{\Delta B}) \quad (4)$$

$$m5 = 0.75 * (\frac{\Delta E}{\Delta B}) \quad (5)$$

The ductility coefficient (m) is calculated based on the equations (1) to (5) in accordance with FEMA356 and ASCE/SEI41-17 provisions. These provisions do not apply to structures with seismic isolation or energy dissipation systems. Composite sections are categorized into C.F.T (Concrete-Filled Tubes) and S.R.C (Steel Reinforced Concrete). Experimental results showed that circular and square sections in C.F.T, and rectangular and square sections in S.R.C, performed best. The geometrical and material properties of these sections were documented. For specimens with cyclic force-displacement curves, the ductility coefficient was determined following additional steps based on Krawinkler-Ibarra's (2005) lateral loading protocol. In finite element modeling using ABAQUS, the results were compared with laboratory data for validation. Finally, statistical analysis (mean, standard deviation, Reliability Test) was applied to determine the ductility coefficient for different performance levels (I.O, L.S, C.P) and for primary and secondary members [26].

3.4. *Ductility Coefficient in C.F.T Sections*

Samples were selected and categorized based on reliable laboratory results. The sections' properties, such as geometric dimensions, material strength, axial load, and the ratio of axial load to nominal capacity, were documented. The ductility coefficient calculation for C.F.T sections depends on the axial load applied and the ratio of section dimension (width or diameter) to thickness. According to FEMA 356 and similar standards, members with an axial load greater than 50% of the nominal capacity are force-controlled, making the ductility coefficient irrelevant. Additionally, references suggest an optimal ratio of 40 to 50 for section dimension-to-thickness for effective concrete-

steel interaction and to distinguish compact from non-compact sections. In this study, a ratio of 40 was adopted as the boundary for C.F.T columns [26].

All the selected samples were subjected to cyclic loading in laboratory experiments conducted by various researchers, and their force-displacement cyclic curves were obtained. In addition to the cyclic curve, other important data, such as absorbed energy, strains at different points, damage and failure modes, the physical condition of the samples after loading, types of deterioration (e.g., strength degradation, stiffness degradation), and other technical aspects, were thoroughly examined and presented [17]. The calculation method for the ductility coefficient in various sections, such as steel, reinforced concrete, and composite sections, is fully explained based on equations 1 to 5 and Figure 4. In the calculation of the ductility coefficient, taking into account the 0.75 factor recommended by the FEMA356 and ASCE/SEI41-17 guidelines, these same references also specify that if the ductility coefficient is less than one, it should be considered as one [27].

3.5. Statistical analysis of the obtained ductility coefficient values

To determine the plasticity indicator coefficient (m) more accurately for composite C.F.T (Concrete-Filled Tube) sections, the experimental specimens were initially categorized into two primary groups based on the section's width-to-thickness ratio: (1) specimens with a ratio less than 40, and (2) specimens with a ratio greater than 40. Within each group, the specimens were further subdivided into four categories according to the level of applied axial load: axial load ratio ≤ 20%, exactly 30%, exactly 40%, and exactly 50%. Subsequently, using statistical relationships and data analysis, the m-values were calculated for each category. The derived coefficients were then compiled and presented. These coefficients have been calibrated in accordance with FEMA 356 guidelines as well as the Iranian National Document No. 360 issued by the Plan and Budget Organization. They are extensively used in linear performance-based analyses of structural systems.

Table 2. Suggested Ductility Coefficient Table for (D/t) Ratios Less Than 40

Week	1. Aerobic Endurance	2. Muscular Endurance	3. Strength	4. Speed-Strength	5. Speed	6. Heart Rate
1	5.60	4.20	2.75	2.10	1.40	<140
2	4.50	3.35	2.70	2.00	1.30	<140
3	3.90	2.90	2.10	1.60	1.10	<140
4	3.40	2.50	1.90	1.40	1.05	<140

Table 3. Suggested Ductility Coefficient Table for (D/t) Ratios Greater Than 40.

Row	D/t Ratio	Axial Load Ratio (%)	m_1 (I.O - Primary)	m_2 (L.S - Primary)	m_3 (L.S - Secondary)	m_4 (C.P - Primary)	m_5 (C.P - Secondary)
1	> 40	10%	4.10	3.10	2.55	1.90	1.25
2	> 40	20%	3.40	2.50	1.80	1.40	1.10
3	> 40	30%	2.65	1.75	1.50	1.25	1.05
4	> 40	40%	1.50	1.35	1.30	1.05	1.00

Tables 2 and 3 summarize the proposed ductility coefficient for C.F.T composite sections, in accordance with FEMA 356 guidelines and its equivalent in the Budget and Planning Organization's Publication 360. This coefficient is widely used in linear analysis based on performance levels. Each row contains the axial load ratio; if the axial load ratio differs from those listed in the rows, the required ductility coefficient (m) can be calculated through linear interpolation. Additionally, it is important to note that for C.F.T sections with an axial load ratio exceeding 50%, the member's behavior will be force-controlled, and the ductility coefficient is no longer applicable. This concept is numerically confirmed as well, as the values converge to one [28].

3.6. Deformation Capacity Factor in S.R.C Sections (Steel Reinforced Concrete)

In this stage, the deformation capacity factor in S.R.C (Steel Reinforced Concrete) sections was calculated and analyzed using valid experimental results from researchers. The samples were categorized and organized based on their geometric characteristics (cross-sectional dimensions and height) and material properties (material strength, axial load,

and its ratio to the nominal axial load capacity). In calculating the deformation capacity factor, important factors such as the applied axial load and the shear reinforcement ratio play a significant role. For sections with exposed concrete surfaces, the distribution of transverse shear reinforcement is particularly crucial.

According to FEMA 356 guidelines, members with an axial load greater than 70% of the nominal capacity of the section are considered force-controlled members, and the deformation capacity factor is not applicable to them. In this study, the maximum acceptable axial load ratio was set at 65%, as increasing the axial load and the lateral strain of steel compared to concrete leads to the formation of extensive cracks in the concrete, which compromises the integrity of the section. This issue is also evident in the extracted tables, where, in this condition, the deformation capacity factor approaches one. Furthermore, the minimum required shear reinforcement was provided and checked according to the ACI318-19, EN.1992.1.1.2004, and EN.1994.1.1.2004 codes for S.R.C sections.

ACI318-19:

$$\rho_{Sv-min}=\frac{A_{Sv-min}}{S*b_w} = \text{Max}\left(\left(\frac{0.062\sqrt{f_c'}}{f_{yt}}\right), \left(\frac{0.35}{f_{yt}}\right)\right) \quad (6)$$

$$\rho_{Sv-min} = \frac{A_{Sv-min}}{S*b_w} = \frac{0.08\sqrt{f_c'}}{f_{yt}} \quad (7)$$

The maximum allowable spacing for shear reinforcements in S.R.C sections is defined by EN.1994.1.1.2004, which selects the smallest value from the following criteria: 20 times the diameter of the smallest longitudinal reinforcement, the minimum dimension of the column section, or 400 mm. Shear cracks typically form diagonally, at a 45-degree angle to the member's longitudinal axis, according to material resistance principles and brittle material behavior [29].

Furthermore, FEMA 356 states that if the spacing of transverse reinforcements exceeds the depth of the section, the member is considered force-controlled and its ductility cannot be verified. Therefore, if the minimum shear reinforcement or maximum spacing criteria are not met, the member is assumed to be force-controlled due to insufficient ductility. Additionally, AISC360-16 (Rev.2019) requires that the spacing of stirrups in S.R.C composite sections should not exceed half the smaller dimension of the column. Samples failing to meet these criteria are excluded from final calculations. In calculating the ductility coefficient, a factor of 0.75, as recommended by the FEMA 356 and ASCE/SEI41-17 standards, is applied. These standards also state that if the ductility coefficient is less than one, it should be considered as one.

3.7. Statistical Analysis of the Obtained Ductility Indicator Coefficients

Initially, the laboratory samples were sorted based on the axial load ratio and categorized into five groups according to different axial load values: less than or equal to 20%, equal to 30%, equal to 40%, equal to 50%, and equal to 65%. Then, using statistical methods and data analysis, the ductility factor for each group was calculated. These tables were prepared using statistical and probabilistic relations to accurately determine the ductility factor, and linear interpolation was enabled for intermediate values. Finally, the ductility factor for S.R.C composite sections was presented according to FEMA 356 standards and the equivalent in Publication 360 of the Planning and Budget Organization of Iran, for linear analysis based on performance levels [30].

Table 4. Proposed Ductility Indicator Coefficient Table for S.R.C Sections

Performance Levels	Axial Load Level	C1	C2	C3	C4	C5	Final Weight
Collapse Prevention (CP)	1.00	1.20	1.75	2.30	2.85	4.00	1
Life Safety (LS)	1.17	1.17	1.70	2.10	2.45	3.15	2
Immediate Occupancy (IO)	1.15	1.15	1.60	2.00	2.25	3.00	3
Operational (O)	1.05	1.05	1.50	1.90	2.10	2.90	4
Fully Operational (FO)	1.00	1.00	1.10	1.50	1.85	2.50	5

In Table 4, the proposed ductility indicator coefficient for S.R.C composite sections is summarized, following the guidelines of FEMA 356 and its equivalent in the publication 360 of the National Budget and Planning Organization. This coefficient is widely applicable in linear analyses based on performance levels. Each row contains the corresponding axial load ratio, and if the axial load is different from the listed values, the required ductility coefficient (m) can be calculated using linear interpolation. A key point to note is that for S.R.C sections with an axial load ratio exceeding

65%, the ductility coefficient reaches a value of one, indicating that the member's behavior is force-controlled, and the ductility coefficient is no longer applicable or meaningful for such sections.

4. Finite Element Modeling

In this study, a set of Concrete-Filled Tube (CFT) composite columns is used for modeling within the Abaqus software environment. For more accurate modeling, concrete is represented using solid elements, while the steel sections are modeled with shell elements. The material properties used in the model include both linear and nonlinear behaviors, which are fully incorporated during the material property definition phase. Additionally, to simulate the connection between welded components, a Tie constraint is applied, and for defining interactions between different surfaces, Surface-to-Surface Contact interaction is employed to properly reflect the real contact conditions between the parts. Detailed information about the geometry, material properties, and other operational parameters of the models used for the CFT column group are provided in Table 5. This data serves as the basis for the model design and forms the foundation for numerical analyses conducted within Abaqus.

Table 5. Specifications of Laboratory C.F.T Sections and Modeled Sections

Performance Level	Axial Load Level (P/Pmax)	C1: Inter-story Drift (%)	C2: Plastic Rotation (rad)	C3: Shear Capacity (kN)	C4: Base Shear (%)	C5: Energy Dissipation (kJ)	Final Weight
Collapse Prevention (CP)	1.00	1.20	1.75	2.30	2.85	4.00	1
Life Safety (LS)	1.17	1.17	1.70	2.10	2.45	3.15	2
Immediate Occupancy (IO)	1.15	1.15	1.60	2.00	2.25	3.00	3
Operational (O)	1.05	1.05	1.50	1.90	2.10	2.90	4
Fully Operational (FO)	1.00	1.00	1.10	1.50	1.85	2.50	5
Service Level - 1 (S1)	1.10	1.10	1.30	1.70	1.95	2.70	6
Service Level - 2 (S2)	1.12	1.12	1.35	1.75	2.00	2.75	7
Service Level - 3 (S3)	1.13	1.13	1.38	1.80	2.05	2.80	8
Service Level - 4 (S4)	1.14	1.14	1.40	1.85	2.10	2.85	9
Service Level - 5 (S5)	1.16	1.16	1.45	1.90	2.15	2.90	10
Enhanced Service (ES)	1.18	1.18	1.50	1.95	2.20	2.95	11
Enhanced Service - High	1.19	1.19	1.55	2.00	2.25	3.00	12
Ultimate Performance (UP)	1.20	1.20	1.60	2.05	2.30	3.05	13

4.1. Results of Modeling C.F.T Column Sample SC.F. T25-1 under Static and Cyclic Loading

After performing the finite element modeling (FEM) of the SC.F. T25-1 sample, which is a C.F.T column, the results are presented in Figure 5. The data is shown as force-displacement curves of the sample under static (uniform incremental) and cyclic loading, along with the skeleton curve, for analysis and comparison.

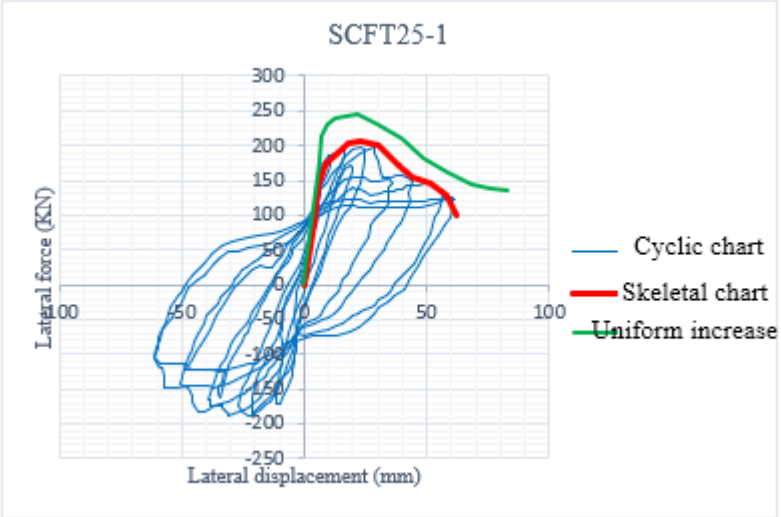

Figure 5. Force-displacement diagram of specimen SC.F.T25-1

4.2. Results of modeling of C.F.T column with the name of specimen SC.F.T25-2 under static and cyclic loading

After modeling by finite element (FEM) of specimen SC.F.T25-2, which is a C.F.T column, the results are presented in Figure 6 in the form of a force-displacement diagram of the said specimen due to static (uniformly increasing) and cyclic loading (along with a skeletal diagram) for review and comparison.

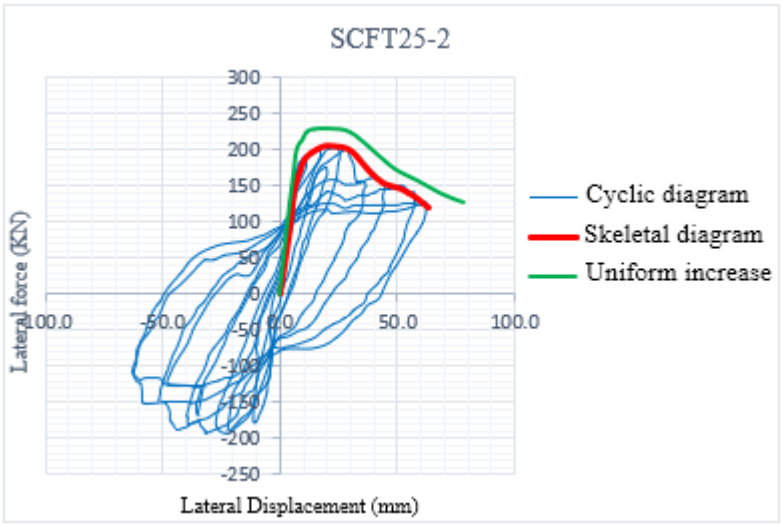

Figure 6. Force-displacement diagram of specimen SC.F.

Due to the same geometric characteristics and materials used, the diagrams of samples SC.F. T25-1 to 4 are very similar to each other and there is no difference in the resulting diagrams, which can be seen in Figures 4 and 5. The differences are less than 5%, which is due to the difference in dimensions of less than 3 mm in the width and depth of the section in these samples (the wall thickness in the samples does not change). However, the matter is slightly different in the case of sample UC.F. T25; because in this sample, a longitudinal stiffener has not been used, which causes deformations in the steel section of the section and reduces the lateral load, which is clearly evident in Figure 5. It should also be noted that in the modeled samples, the amount of axial load applied is zero.

4.3. Results of modeling of C.F.T column with the name of specimen UC.F. T25 under static and cyclic loading

As mentioned earlier, longitudinal stiffener is not used in this specimen. Therefore, the lateral force-displacement diagram resulting from modeling of this specimen is different from the specimens SC.F. T25-1~4. After modeling by finite element (FEM) of specimen UC.F. T25 which is a C.F.T column, the results are presented in Figure 7 as a force-displacement diagram of the specimen resulting from static (uniformly increasing) and cyclic loading (along with skeletal diagram) for review and comparison.

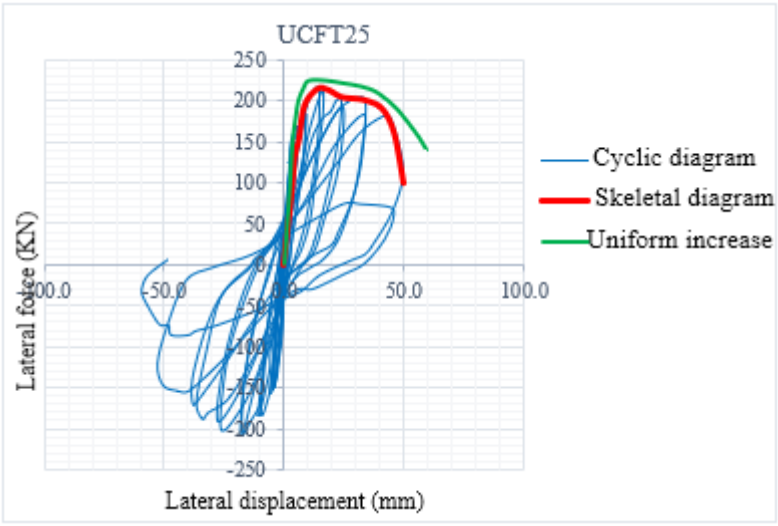

Figure 7. Force-displacement diagram of sample UC.F.T25

As is clear from comparing the graphs above, the specimen's ductility, maximum lateral displacement, and maximum tolerable lateral force have decreased significantly. The rings in the graph have also become narrower. Therefore, the role of longitudinal stiffening in the ductility of C.F.T. sections and also the tolerable lateral force is quite evident and effective, as in conventional traditional steel sections. Considering the low weight and much lower relative cost, doing this, in addition to its very good structural role, also has a completely positive effect on making C.F.T. sections more economical.

4.4. Results of modeling of C.F.T column with the name of sample SC.F.T19-1~3 under static and cyclic loading

After modeling by finite element (FEM) of sample SC.F.T19-1, which is a C.F.T column, the results are presented in Figure 8 in the form of force-displacement diagram of the said sample due to static (uniformly increasing) and cyclic loading (along with skeletal diagram) for review. Considering the same geometric specifications and materials used, the diagrams of samples SC.F.T19-1 to 3 are very similar to each other and there is no difference in the resulting diagrams. The differences are less than 5%, which is due to the difference in dimensions of less than 3 mm in the width and depth of the section in these samples (the wall thickness in the samples does not change).

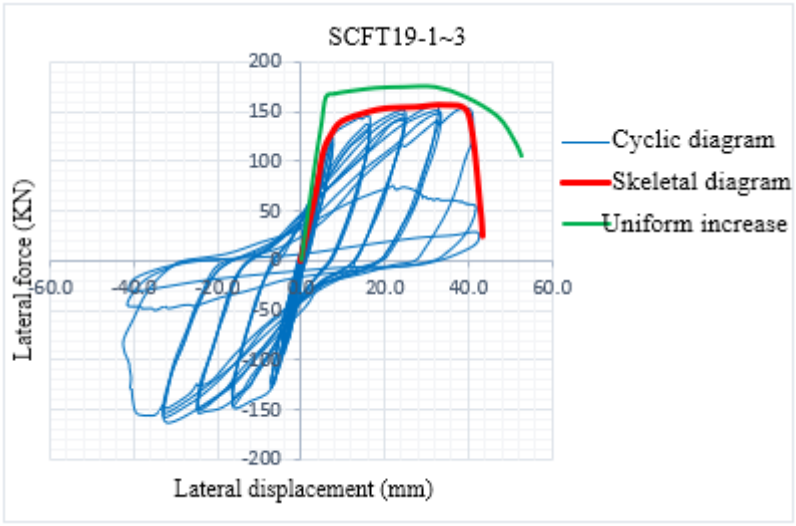

Figure 8. Force-displacement diagram of samples SC.F.T19-1~3

It is worth noting that the samples of the SC.F.T19-1~3 series have a shorter length than the samples of the SC.F.T25-1~4 series. Also, the ratio of the cross-sectional dimension to its thickness ($\frac{D \text{ or } B}{t}$) is also lower and is equal to 76. Therefore, the ductility of these samples is higher than that of the aforementioned series.

4.5. Results of modeling of C.F.T column with the name of sample SC.F. T13-1~4 under static and cyclic loading

After modeling by finite element (FEM) of sample SC.F. T13-1, which is a C.F.T column, the results are presented in Figure 9 in the form of force-displacement diagram of the said sample due to static (uniformly increasing) and cyclic loading (along with skeletal diagram) for review. Considering the same geometric specifications and materials used, the diagrams of samples SC.F. T13-1 to 4 are very similar to each other and there is no difference in the resulting diagrams. The differences are less than 5%, which is due to the difference in dimensions of less than 3 mm in the width and depth of the section in these samples (the wall thickness in the samples does not change).

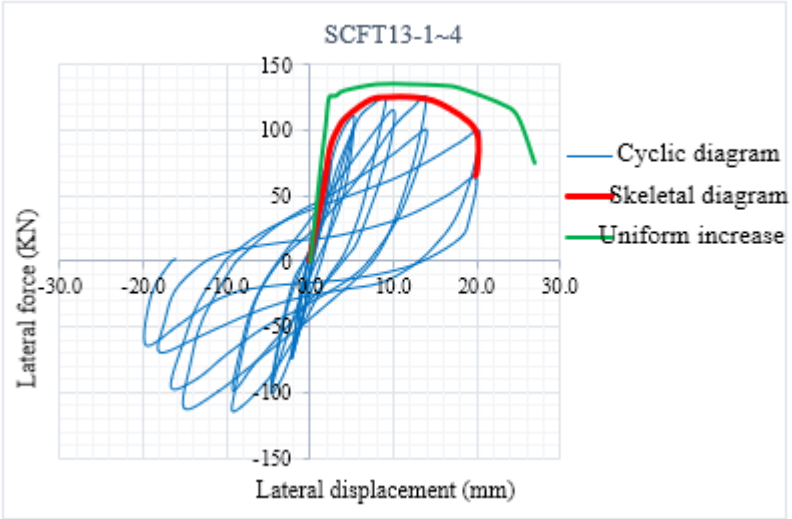

Figure 9. Force-displacement diagram of samples SC.F.T19-1~3

It is worth noting that the samples of the SC.F.T13-1~4 series have a shorter length than the samples of the SC.F.T19-1~3 series. Also, the ratio of the cross-section to its thickness ($\frac{D \text{ or } B}{t}$)is also lower and is equal to 52. Therefore, the ductility of these samples is higher than that of the aforementioned series, which numbers have been examined in detail in the table at the end of this section.

4.6. Results of modeling of C.F.T column with the name of specimen UC.F.T13 under static and cyclic loading

As mentioned earlier, longitudinal stiffener is not used in this specimen. Therefore, the lateral force-displacement diagram resulting from modeling of this specimen is different from the specimens SC.F.T13-1~4. After modeling by finite element (FEM) of specimen SC.F. T13-1 which is a C.F.T column, the results are presented in Figure 10 in the form of force-displacement diagram of the said specimen resulting from static (uniformly increasing) and cyclic loading (along with skeletal diagram) for review and comparison.

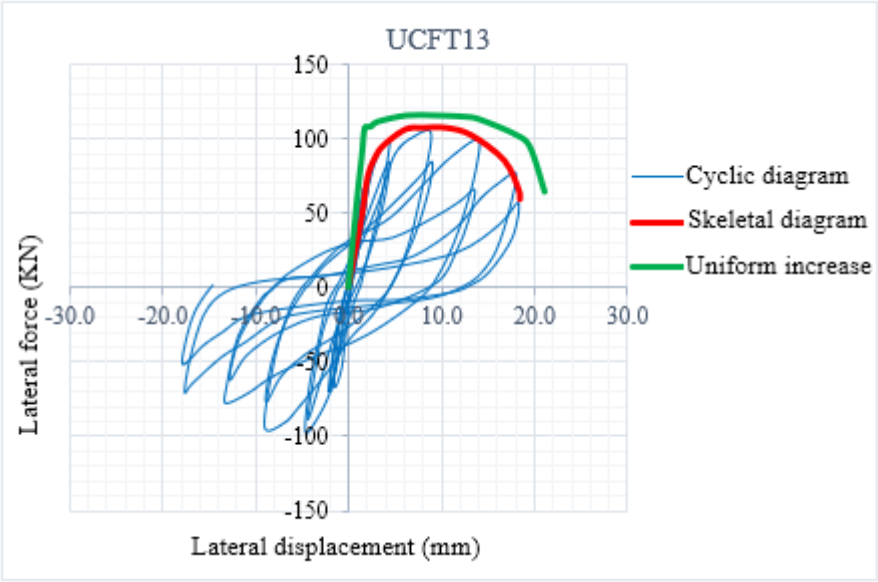

Figure 10. Force-displacement diagram of sample UC.F.T13

As can be seen from the comparison of the graph in Figure 10 with the graphs in Figure 9, the ductility of the sample, maximum lateral displacement, and maximum tolerable lateral force have decreased significantly. The rings in the graph have also become narrower. Therefore, the role of longitudinal stiffening in the ductility of C.F.T. sections and also the tolerable lateral force is quite evident and effective, as in conventional traditional steel sections. Considering the low weight and much lower relative cost, doing this, in addition to its very good structural role, also has a completely positive effect on making C.F.T. sections more economical.

4.7. Investigation and calculation of energy absorbed by C.F.T composite sections

After identifying and investigating the factors and parameters affecting the amount of energy absorbed by C.F.T composite sections, this section examines the combined effect of these factors on the amount of energy absorbed by the sections and finally presents a relationship to predict the energy absorbed by C.F.T composite sections.

At this stage, first, 5 parameters from the parameters listed in the aforementioned sections were selected and a statistical relationship was established, followed by curve fitting between these points and the energy absorbed by the samples, the result of which is proposed in Equations 8 and 9. The output of this equation is presented in Figure 7 in the form of a graph. It should be noted that due to the different implementation details used in the samples, the results have some deviation. These operational differences can be attributed to different support conditions, welding details in the joints, use or non-use of stiffeners in some samples, and other such cases; but in general, the fitted diagram and the proposed relationship provide a very strong view of the exact effect of each factor on the energy absorbed by the examined samples, which can be used as an indicator in the design path.

In the diagram below, there are two groups of points with different colors. One of them (red color) corresponds to the results obtained from the laboratory and the other group (blue color) is the points obtained from the proposed relationship Nos. 8 and 9. Another point is that the exponential trend line of each data set is also drawn on the diagram with the same color and as a dotted line, which indicates a complete correlation between the points of the two groups.

$$C = 0.28\ t + 0.021\ (\frac{D}{t}) + 0.48\ (\frac{L}{D}) + 0.02\ f'_C - 0.1\ P + 2.3 \quad (8)$$

$$E = f(C) = EXP(C) \quad (9)$$

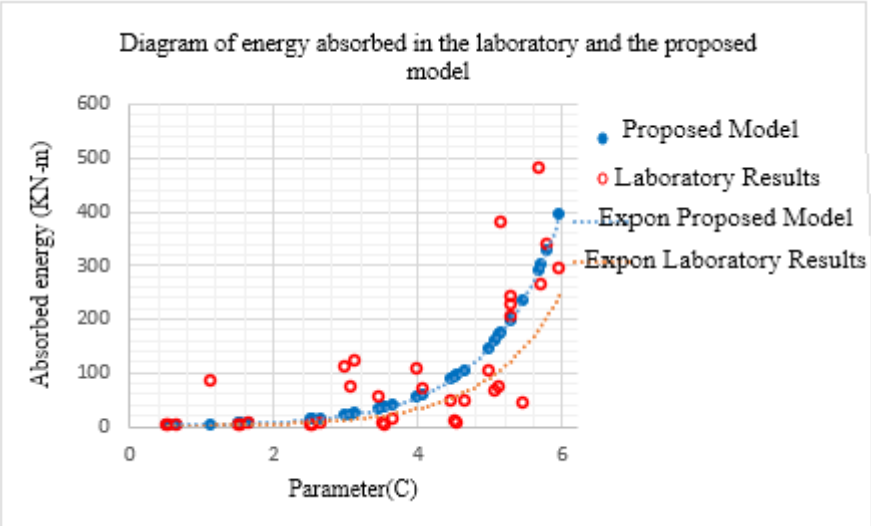

Figure 11. Relationship diagram between parameter C and amount of absorbed energy (in two experimental cases and proposed model)

5. Discussion and Conclusion

In order to obtain the ductility coefficient of composite sections, 85 samples were selected in C.F.T type composite sections and 54 samples in S.R.C type composite sections, and after examining their laboratory cyclic diagrams, tables were presented for each group to calculate the ductility coefficient. In the case of C.F.T sections, the samples were classified into two general groups with a ratio of section dimension to steel thickness less than and more than 40 times. In each of the samples, the ranges of axial load ratio were divided into percentage steps and samples were selected in C.F.T sections up to 50% ratio and in S.RC sections up to 65% ratio of compressive axial load. In each of these groups, at the upper limit of the axial load ratio, the ductility coefficient tended towards unity (one), which indicates the transformation of the member state from being controlled by deformation to being controlled by force. Another point is that the ductility coefficient in C.F.T sections has performed better and more than in S.R.C sections. Another important point is that in the case of S.R.C sections, in addition to the axial load ratio, the amount of transverse reinforcement and their spacing also have a great effect on the ductility of the member and its ductility coefficient.

After completing the previous stage, in the study of the axial load-bearing capacity of composite sections based on the results obtained from the laboratory and the EC.4 and AISC360-2005 relations, 230 C.F.T samples and 89 S.R.C samples were selected in each type of section. Based on the calculations of material strength and statistical work, a relation was presented for each type of section (C.F.T or S.R.S) to predict the axial load-bearing capacity. Its results were examined with the two aforementioned regulations and matched with the laboratory results. It was found that the proposed relations in this study performed more desirable and better than the two aforementioned regulations in terms of both the quantity and number of samples and the quality of predicting the axial load-bearing capacity. After completing the two aforementioned stages, a number of laboratory samples whose axial loading results were only available were selected and modeled and matched with the ABAQUS finite element software. After verifying and matching the results, which confirmed the correct performance of the software model, the samples were subjected to lateral loading with the lateral loading protocol proposed by Krawinkler-Ibarra and their cyclic curves were extracted. After extraction, the ductility coefficients were calculated for these samples and adjusted in the relevant tables. It is worth noting that the axial load capacity of the aforementioned samples was calculated based on the proposed relationship in the present study and was matched with the laboratory results and two other regulations, which again showed the appropriate performance of the proposed relationship.

Next, the parameters affecting the amount of energy that can be absorbed by C.F.T. composite sections were examined. After determining the effect of each parameter, a general relationship was developed and expanded to include all the influencing items, which was matched with the laboratory results in the relevant diagram. As mentioned earlier, due to different implementation details in the

construction of the studied samples, the results from the proposed relationship and the laboratory results in the calculation of the energy absorbed by C.F.T. sections have a slight dispersion, but the overall trend of both cases (laboratory and proposed model) has a very high agreement, which can indicate the factors affecting the amount of energy absorbed, which correctly declares the cases. In this regard, the way and direction of the effect of each factor on the amount of energy absorbed can be predicted and examined.

Authors' Contributions

Authors equally contributed to this article.

Acknowledgments

Authors thank all participants who participate in this study.

Declaration of Interest

The authors report no conflict of interest.

Funding

According to the authors, this article has no financial support.

Ethical Considerations

All procedures performed in this study were under the ethical standards.

References

[1] S. Han *et al.*, "Simplified equivalent design for novel hybrid steel-FRP composite bars and closed-type FRP stirrups reinforced seawater sea-sand concrete columnsJO - Engineering Structures," vol. 331, p. 119995, 2025, doi: 10.1016/j.engstruct.2025.119995.

[2] H. Yuan, H. P. Hong, H. Deng, and Y. Bai, "Displacement ductility of staged construction-steel tube-reinforced concrete columns," *Construction and Building Materials*, vol. 188, pp. 1137-1148, 2018, doi: 10.1016/j.conbuildmat.2018.08.141.

[3] T. Zhou, M. Xu, Z. Chen, and Y. Li, "Experimental study on biaxial eccentric compression stability of L-shaped special-shaped columns composed of concrete-filled square steel tube connected by steel plates," *Build. Struct.*, vol. 48, pp. 82-86, 2018.

[4] J. Zeghiche and K. Chaoui, "An experimental behaviour of concrete-filled steel tubular columns," *J. Constr. Steel Res.*, vol. 61, pp. 53-66, 2005, doi: 10.1016/j.jcsr.2004.06.006.

[5] S. Ghannam, "Buckling of Concrete-Filled steel tubular slender columns," *Int. J. Res. Civ. Eng. Archit. Des.*, vol. 3, pp. 41-47, 2015.

[6] F. Zhang, X. Liu, F. W. Ge, and C. Cui, "Investigation on the Ductility Capacity of Concrete Columns with High Strength Steel Reinforcement under Eccentric Loading," *Materials*, vol. 16, no. 12, p. 4389, 2023, doi: 10.3390/ma16124389.

[7] S. M. Zhou *et al.*, "Determining experimental ductile behavior of composite walls considering second-order effects: A case study for multi-celled CFST walls Experimental study and numerical simulation of a new prefabricated SRC column to steel beam composite joint," 2023, vol. 57, pp. 105121-1010, doi: 10.1016/j.istruc.2023.105121 10.1016/j.istruc.2020.06.027.

[8] Q. H. Li, C. J. A. U. L. J. F. Sun, G. Quan, B. T. Huang, and S. L. Xu, "Fire performance of steel-reinforced ultrahigh-toughness cementitious composite columns: Experimental investigation and numerical analyses," *Journal of Structural Engineering*, vol. 146, no. 3, p. 04020012, 2020, doi: 10.1061/(ASCE)ST.1943-541X.0002567.

[9] B. L. Lai, R. L. Bao, M. Y. Zhang, Y. H. Wang, and J. R. Liew, "Evaluation on the static and seismic performance of steel reinforced concrete composite columns with high strength materials," *Journal of Building Engineering*, vol. 79, p. 107886, 2023, doi: 10.1016/j.jobe.2023.107886.

[10] S. M. Saleh and A. L. A. İhsan, "Strength and behaviour assessment of axially loaded concrete filled steel tubular stub columns," *Turk. J. Eng.*, vol. 5, pp. 154-164, 2021, doi: 10.31127/tuje.686246.

[11] S. Jayalekshmi and J. S. Sankar Jegadesh, "Finite Element Analysis and Codal Recommendations of Concrete Filled Steel Tubular Columns," *J. Inst. Eng. Ser. A*, vol. 97, pp. 33-41, 2016, doi: 10.1007/s40030-016-0144-4.

[12] A. M. Heman and K. G. Roshni, "Numerical Study on Concrete-Filled Steel Tubes with Diagonal Binding Ribs and Longitudinal Stiffeners." Singapore: Springer, 2022, pp. 15-24.

[13] B. Grzeszykowski and E. D. Szmigiera, "Experimental investigation on the vertical ductility of rectangular CFST columns loaded axially," *Materials*, vol. 15, no. 6, p. 2231, 2022, doi: 10.3390/ma15062231.

[14] W. J. Peng and M. X. Tao, "Column-to-beam flexural strength ratio for rigorous strong-column-weak-beam design for steel-concrete composite frames," *Journal of Building Engineering*, vol. 96, p. 110669, 2024, doi: 10.1016/j.jobe.2024.110669.

[15] W. Sun and S. Li, "Mechanical property analysis and calculation method modification of steel-reinforced high-strength concrete columns," *Materials*, vol. 15, no. 19, p. 6863, 2022, doi: 10.3390/ma15196863.

[16] P. Chen, Z. Chen, Z. Guo, T. Wang, and W. Yang, "Experimental studies on the axial compression performance and bearing capacity of pultruded GFRP tube-concrete-round steel tube double-skin hollow columns," 2025, vol. 71, p. 108100, doi: 10.1016/j.istruc.2024.108100.

[17] S. Azad, S. R. Mirghaderi, and S. Epackachi, "Numerical investigation of steel and composite beam-to-encased composite column connection via a through-plate," 2021, vol. 31, pp. 14-28, doi: 10.1016/j.istruc.2021.01.040.

[18] P. Katsimpini, G. Papagiannopoulos, and G. Hatzigeorgiou, "An In-Depth Analysis of the Seismic Performance Characteristics of Steel-Concrete Composite Structures," *Applied Sciences*, vol. 15, no. 7, p. 3715, 2025, doi: 10.3390/app15073715.

[19] L. Zhou and S. Yi-sheng, "Experimental study on seismic behavior of SRC deep beam-to-CFST column frames," *Journal of Constructional Steel Research*, vol. 155, pp. 157-175, 2019, doi: 10.1016/j.jcsr.2018.12.014.

[20] M. Fukuhara and K. Minami, "Seismic performance of new type steel-concrete composite structures considering characteristic both SRC and CFT structures," 2008.

[21] R. Bhartiya and D. R. Sahoo, "Prediction of axial compression behavior of rectangular RCFST columns with confining ties," *J. Constr. Steel Res.*, vol. 186, p. 106920, 2021, doi: 10.1016/j.jcsr.2021.106920.
[22] S. H. Boukhalkhal, L. F. D. C. Neves, and W. Madi, "Dynamic behavior of concrete filled steel tubular columns," *Int. J. Struct. Integr.*, vol. 10, pp. 244-264, 2019, doi: 10.1108/IJSI-07-2018-0040.
[23] A. Lazkani, "Behavior of Expansive Concrete-Filled Steel Tubular (Ecfst) Columns under Axial Loadings," 2016. [Online]. Available: https://scholarworks.uaeu.ac.ae/all_theses/316.
[24] V. W. Y. Tam, Z. Tao, and A. Evangelista, "Performance of recycled aggregate concrete filled steel tubular (RACFST) stub columns with expansive agent," *Constr. Build. Mater.*, vol. 272, p. 121627, 2021, doi: 10.1016/j.conbuildmat.2020.121627ER -.
[25] S. Ahmad, K. Kumar, and A. Kumar, "Axial behaviour of steel tubes filled with concrete incorporating high-volume rubber," *Innov. Infrastruct. Solut.*, vol. 7, p. 148, 2022, doi: 10.1007/s41062-022-00739-6.
[26] X. Li, J. Liu, X. Wang, and Y. F. Chen, "Assessment on the seismic performance of circular tubed reinforced concrete column to steel beam frames using numerical modeling," *Soil Dynamics and Earthquake Engineering*, vol. 163, p. 107567, 2022, doi: 10.1016/j.soildyn.2022.107567.
[27] R. Pang, W. Wang, F. Zhou, and S. Ding, "Experimental and analytical investigation on the compressive behavior of double-skin steel-concrete composite tube walls," *Journal of Building Engineering*, vol. 73, p. 106681, 2023, doi: 10.1016/j.jobe.2023.106681.
[28] D. Ahiwale, R. Khartode, A. Bhapkar, G. Narule, and K. Sharma, "Influence of compressive load on concrete filled steel tubular column with variable thickness," *Innov. Infrastruct. Solut.*, vol. 6, p. 23, 2021, doi: 10.1007/s41062-020-00390-z.
[29] P. Achuthan, G. G. Prabhu, G. G. Vimal Arokiaraj, P. A. Sivanantham, and S. Suthagar, "Axial Compression Performance of Concrete-Filled Steel Tubular Columns with Different D/t Ratios," *Adv. Mater. Sci. Eng.*, vol. 2022, p. 9170525, 2022, doi: 10.1155/2022/9170525.
[30] N. Umamaheswari and S. Arul Jayachandran, "Experimental Investigation on Uniaxial Compressive Behaviour of Square Concrete Filled Steel Tubular Columns." New Delhi, India: Springer, 2015, pp. 2087-2101.